Estimate of the EXO-200 Radon Production Inside the TPC

A. Piepke and K. Pushkin

University of Alabama

12/21/2011

Abstract

The steady state Radon emanation from the EXO-200 TPC body and its internals has been studied. Radon release by nuclear recoil and diffusion was taken into account. The temperature dependence of diffusivities was evaluated and incorporated into the model. The outgassing estimates assume U-chain equilibrium and make use of the measured radioactivity content of all components.
Based on this analysis we estimate that the TPC can support a steady state Radon population of 3.9 atoms at 167 K and of 243 atoms at 298 K. Because of the semi-quantitative nature of some of the estimates, a reasonable confidence range would be a tenth up to ten times the yields given. Even with these rather wide error bands it seems that the population of 200 radon atoms in the EXO-200 Xenon cannot be sustained by internal TPC radioactivity. Possible and unknown U-surface activities have not been taken into account. This is an additional element of uncertainty.

1 Motivation

This study is motivated by the question whether or not the steady state population of about 200 ^{222}Rn atoms in the active xenon of EXO-200 can be supported by outgassing of TPC components. The question whether or not the Radon source is external or internal is important for our planning for a Radon trap.
The ^{238}U concentrations or stringent limits for it are known from our pre-assembly material testing. The assumption of radioactive chain equilibrium

directly relates the ^{238}U decay rate, R_U, to that of ^{222}Rn, abbreviated as R_{Rn}, such that:

$$\begin{aligned} R_U &= R_{Rn} \\ \Rightarrow N_{Rn} &= \frac{\tau_{Rn}}{\tau_U} \cdot N_U \;=\; \tau_{Rn} \cdot R_U, \end{aligned}$$

where N_U and N_{Rn} denote the number of U and Rn atoms in each detector component. τ_U and τ_{Rn} stand for the mean live times of of U and Rn. Knowledge of the ^{238}U concentration, c_i (in units of g/g), of component i with mass, m_i, and the equilibrium assumption allows us to estimate the number of Rn atoms present in steady state in each detector component:

$$N_{Rn,i} \;=\; \alpha \cdot c_i \cdot m_i \cdot \tau_{Rn},$$

where $\alpha = 12.35 \cdot 10^3 \; \frac{1}{s\,g}$ denotes the (mass) specific ^{238}U activity. In equilibrium the production rate, n_i, of Radon per unit volume, V_i in sample i, relates to the ^{238}U mass concentration:

$$\begin{aligned} n_i &= \frac{R_{U,i}}{V_i} \\ c_i &= \frac{m_{U,i}}{m_{s,i}} \\ &= \frac{R_U}{\alpha \cdot \rho_i \cdot V_i} \\ &= \frac{n_i}{\alpha \cdot \rho_i} \\ \Rightarrow n_i &= \alpha \cdot \rho_i \cdot c_i, \end{aligned}$$

where $m_{s,i}$ and $m_{U,i}$ denote the sample and U-mass of component i. n_i has unit $\frac{1}{s \cdot cm^3}$ and describes the Radon production yield per unit sample volume. It is the source term that powers Radon outgassing.
For parts where the U-content is specified per unit surface area, c_i', one needs to know their thickness H_i to get:

$$\begin{aligned} c_i &= \frac{c_i'}{H_i \cdot \rho_i} \\ \Rightarrow n_i &= \frac{\alpha \cdot c_i'}{H_i} \end{aligned}$$

In order to quantify the Rn outgassing of TPC components, we further need to know the fraction of atoms escaping their host into the xenon.

Material	Amount	Unit	^{238}U content	Unit	Volume $[cm^3]$	Area $[cm^2]$	^{222}Rn content $[atoms]$	^{222}Rn yield $[atoms/day]$
External Cu	29668	g	$< 3.8 \cdot 10^{-12}$	g/g	3329	39050	< 664	< 120
Internal Cu	10012	g	$< 3.8 \cdot 10^{-12}$	g/g	1123	12120	< 224	< 41
Phosphor-bronze	407	g			45.7	4130		
APDs	468		$< 1.7 \cdot 10^{-11}$	g	137	3795	< 46	< 8.4
Acrylic	1460	g	$< 4 \cdot 10^{-12}$	g/g	1230	7340	< 34	< 6.2
0.028" PTFE	4625	g	$< 4 \cdot 10^{-13}$	g/g	2013	43420	< 11	< 2
0.060" PTFE	280	g	$< 4 \cdot 10^{-13}$	g/g	121	1664	< 0.7	< 0.12
Flat cables	37600	cm^2	$(5.7 \pm 0.7) \cdot 10^{-12}$	g/cm^2	43.3	37600	1260 ± 155	229 ± 3

Table 1: Material amounts, analysis results, and Radon production estimates. Only the ^{238}U analysis results and the associated ^{222}Rn production yields are listed assuming secular chain equilibrium.

2 Material and Activity Accounting

The amounts of the various materials used for the assembly of the TPC are known. Table 1 lists the different construction materials and components along with their mass, volume, surface area, and U content. Mass and dimensional data of all components was obtained from a 3D detector model maintained by Matt Swift of SLAC. The table further lists the Radon production yield, as determined from the equilibrium hypothesis. The flat cables are the largest reservoir of Radon. The flat cables have a thickness of only 25 μm which will allow some Radon escape. If all Radon contents are set to their upper limit values, the total Radon inventory of the TPC components is estimated to be 2280 atoms. This number is not small compared to the 200 Radon atoms contained in the xenon in steady state. The release has to be considered more carefully in order to understand whether TPC components could be significant contributors to the internal Radon inventory.

3 Radon Release from Materials

3.1 General Considerations

^{222}Rn is born in α-decay of ^{222}Ra. The nuclear recoil energy is about 85 keV. Nuclear recoil and diffusion are the two principal ways for Rn to escape its host material.

1. Nuclear recoil: the moving atom is highly ionizing. This results in an extremely low range in a dense medium. Based on an estimate by the Borexino collaboration [1] the recoil induced displacement of Rn atoms is of order 30 nm. We evaluate the recoil ion range using the simulation code SRIM/TRIM (version 2008.04). For the EXO-200 outgassing estimate we will take the material specific ranges $\ell_{max,i}$ to be the thickness of the production volume and assume that one quarter of all Rn atom born in this layer will by ejected into the xenon. For metals this is the principal Radon release mechanism.

2. Diffusion: also based on [1] we assume that Radon diffusion in metals is negligible. We couldn't find any measured diffusion coefficients for noble gases in metals. However, Radon is mobile in plastics and diffusion coefficients can be found in the literature. These are typically

measured at room temperature. The estimates of Radon outgassing from plastic components presented here are based on solving the diffusion equation. For plastics at room temperature this is the principal Radon release mechanism.

3.2 Recoil Driven Release of Radon

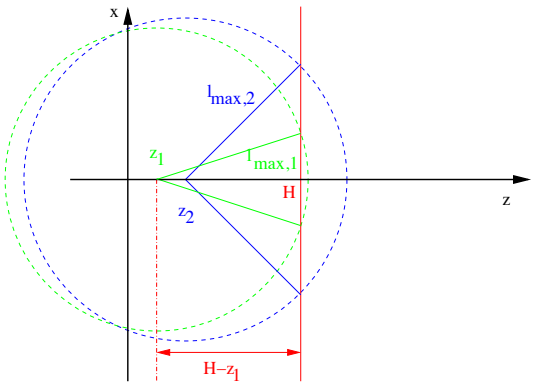

Figure 1: Solid angle available to recoiling Radon atoms within range of a surface.

For a given range ℓ_{max} of a recoiling Radon atom in a host material the fraction f of all atoms born within one range of the nearest surface will be ejected from the host material. It is assumed here that $H \gg \ell_{max}$, assuring that only one surface can contribute to the escape fraction for any decay. Figure 1 depicts this situation. For a decay location z within the range $H - \ell_{max} < z < H$ the half opening angle of the emission cone is determined by the particle range:

$$\theta_{max} \;=\; \arccos\left(\frac{H-z}{\ell_{max}}\right)$$

The fractional solid angle (spherical surface area), $\Omega(z)$, available for emission outside the membrane is given by:

$$\begin{aligned}
\Omega(z) &= \frac{\int_{\phi=0}^{2\cdot\pi}\int_{\theta=0}^{\theta_{max}} \ell_{max}^2 \cdot sin\theta \; d\theta \; d\phi}{4\cdot\pi\cdot\ell_{max}^2} \\
&= \frac{\ell_{max}^2\cdot 2\cdot\pi}{\ell_{max}^2\cdot 4\cdot\pi}\cdot\int_{\theta=0}^{\theta_{max}} sin\theta \; d\theta \\
&= \frac{1}{2}\cdot[-\cos\theta]_0^{\theta_{max}} \;=\; \frac{1}{2}\cdot(1-\cos\theta_{max}) \\
&= \frac{1}{2}\cdot\left(1-\frac{H-z}{\ell_{max}}\right) \qquad (1)
\end{aligned}$$

ϕ and θ denote the azimuthal and zenith angle. θ is taken relative to the z-axis and thus half the opening angle of the acceptance cone. One can see from equation 1 that the fractional solid angle depends linearly on the decay position z.
One must now average over all possible decay locations to get f. The integration over all allowed locations does not require any weighing by squares of distances to the surface. All spheres, representing the solid angle of a particular location, have the same radius ℓ_{max}. The solid angle restriction is solely determined by the opening angle of the acceptance cone, shown in figure 1. Using this summing f is given as:

$$\begin{aligned} f &= \frac{\int_{z_{min}}^{z_{max}} \Omega(z)\, dz}{\int_{z_{min}}^{z_{max}} 1\, dz} \\ &= \frac{\frac{1}{2} \cdot \int_{H-\ell_{max}}^{H} 1 - \frac{H-z}{\ell_{max}}\, dz}{H - (H - \ell_{max})} \\ &= \frac{1}{2 \cdot \ell_{max}} \cdot \left[\left(1 - \frac{H}{\ell_{max}}\right) \cdot \ell_{max} + \frac{1}{\ell_{max}} \cdot \left[\frac{z^2}{2}\right]_{H-\ell_{max}}^{H} \right] \\ &= \frac{1}{2} \cdot \left[1 - \frac{H}{\ell_{max}} + \frac{2 \cdot H - \ell_{max}}{2 \cdot \ell_{max}}\right] = \frac{1}{4} \end{aligned} \tag{2}$$

This estimate indicates that one quarter of the Radon atoms emitted within a surface skin of thickness ℓ_{max} is ejected into the outside medium. The

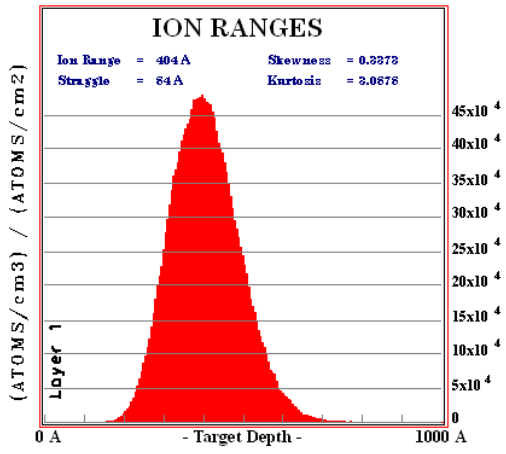

Figure 2: Range of Rn-ions in PTFE as calculated by a SRIM-simulation. The range straggling is shown in the width of the peak.

range of recoiling *Rn* ions with a kinetic energy of 85 keV has been calculated using SRIM. Such calculation was done for Kapton, Acrylic, PTFE, silicon, copper, and phosphor-bronze. Figure 2 shows the longitudinal range and

range-straggling obtained for PTFE. Room temperature densities have been used and it has been assumed that the recoil release is, to lowest order, independent of temperature.

Material	Longitudinal range $[nm]$	Longitudinal straggling $[nm]$
Kapton	58.5	8.3
Acrylic	65.0	8.9
PTFE	40.5	6.7
Silicon	42.3	9.0
Copper	14.1	4.6
Phosphor-bronze	14.6	4.9

Table 2: Range of singly charged 85 keV Radon ions, as determined by a SRIM simulation.

The dependence of the range on the Radon ion charge state has not been explored. It is to be expected that the Radon ions exist in a variety of charge states. However, we do not have data on the composition of this mix of states. For this estimate it was *assumed* that all ions are singly charged. Table 2 lists the ranges and straggling obtained this way for all relevant materials. For the outgassing estimates the range was used. We make no use of the range straggling.

3.3 Diffusion Driven Outgassing by a Membrane

In this section we will treat the Rn outgassing problem. However, at the cryogenic temperatures of EXO-200 Rn outgassing is described by the simple expression given in equation 8. Readers not interested in the mathematical details may skip to the next section.

The problem of Radon diffusion through thin membranes has been treated in several publications, for example [2, 3]. However, these results are not directly applicable to our situation. Reference [4] treats the outgassing problem, however, in a time dependent way. We are here treating the steady state situation, resulting in a considerable simplification of the mathematical expressions, compared to those given in [4].
Let $u(x,t)$ be the Radon number concentration inside the membrane, let D be the Radon diffusion constant (diffusivity) of the membrane material, and

let λ be the Radon decay constant. $u(x,t)$ is determined by the diffusion equation and the boundary conditions. The problem is treated as one dimensional transport, this is valid for thin samples (like most plastics in the EXO-200 TPC). This approach is typically also chosen for problems involving diffusion through a membrane [2, 3]. Figure 3 depicts the situation. We assume that there is no radon in the medium surrounding the membrane and that inside the membrane there is a initially homogeneous distribution.

1. $x = 0$ and $t = 0$, $u(x,t) = 0$
2. $x = H$ and $t = 0$, $u(x,t) = 0$
3. $0 < x < H$ and $t = 0$, $u(x,t) = C = constant$

It is further assumed that for all times the Radon concentration for $x < 0$ and $x > H$ remains zero, or in other words that the external reservoir is infinitely large compared to the outgassing membrane. Given the mass ratio of Xenon to all internal plastics used in EXO-200 this seems a good approximation. The estimated steady state Radon concentration in Kapton is about 29 $atoms/cm^3$, as can be seen from table 1. This is about 7000 time larger than the measured concentration of Radon atoms in the TPC xenon.
Radon is being produced inside the membrane at a constant rate n (in $\frac{atoms}{cm^3\ s}$) due to its internal U-content. The Radon concentration is, thus, described by a modified diffusion equation:

$$D \cdot \frac{\partial^2 u(x,t)}{\partial x^2} - \lambda \cdot u(x,t) + n \ = \ \frac{\partial\ u(x,t)}{\partial t} \tag{3}$$

Although the boundary conditions demand the Radon concentration to be zero at all times at the membrane boundaries, a useful expression for the Radon flux at $x = 0$ and $x = H$ is obtained by evaluating the rate of change of the concentration at the boundaries [2, 3]:

$$\Phi \ = \ D \cdot \frac{\partial\ u(x,t)}{\partial x}|_{x=0,H} \tag{4}$$

Note that Φ, as defined in equation 4, has dimension $\frac{atoms}{cm^2\ s}$ as required for a flux.

Solving equation 3 is possible (by separation of variables) but not necessary. We are not really interested to model the full time dependence of the outgassing. Getting a useful expression for the *steady state* outgassing

is sufficient. Equilibrium has been achieved whenever the Radon concentration doesn't change any more or $\frac{\partial\, u(x,t)}{\partial t} = 0$. In steady state equation 3 has no more time dependence. In this limit the Radon concentration function becomes one dimensional $u(x,t) \rightarrow u(x)$ and equation 3 becomes an ordinary differential equation in space:

$$D \cdot \frac{d^2u(x)}{dx^2} - \lambda \cdot u(x,t) + n \;=\; 0 \tag{5}$$

Equation 5 is solved by:

$$u(x) \;=\; A \cdot e^{\sqrt{\frac{\lambda}{D}} \cdot x} + B \cdot e^{-\sqrt{\frac{\lambda}{D}} \cdot x} + \frac{n}{\lambda} \tag{6}$$

As discussed before we are assuming the Radon concentration to vanish at the membrane boundaries: $u(0) = u(H) = 0$. With these boundary conditions the constants of integration are:

$$\begin{aligned} A &= -\frac{n}{\lambda} \cdot \frac{1 - e^{-\sqrt{\frac{\lambda}{D}} \cdot H}}{2 \cdot \sinh(\sqrt{\frac{\lambda}{D}} \cdot H)} \\ B &= -A - \frac{n}{\lambda} \;=\; -\frac{n}{\lambda} \cdot \left[1 - \frac{1 - e^{-\sqrt{\frac{\lambda}{D}} \cdot H}}{2 \cdot \sinh(\sqrt{\frac{\lambda}{D}} \cdot H)} \right] \end{aligned}$$

Using equation 4 one obtains the steady state Radon out-flux as:

$$\Phi \;=\; n \cdot \sqrt{\frac{D}{\lambda}} \cdot \left[1 - \frac{1 - e^{-\sqrt{\frac{\lambda}{D}} \cdot H}}{\sinh(\sqrt{\frac{\lambda}{D}} \cdot H)} \right] \tag{7}$$

For plastics *at room temperature* Radon diffusion constants found in the literature [2, 3, 5] range from 10^{-7} to 10^{-12} $\frac{cm^2}{s}$. Depending on the material the diffusion time constant $\frac{H^2}{D}$ ranges from 0.3 d to 290 d for the Kapton cables (with $H = 0.005\ cm$). This indicates that equilibrium might not yet be established in some EXO materials. The typical outgassing length scale is $\ell = \sqrt{\frac{D}{\lambda}}$. For $D = 5 \cdot 10^{-12}$ $\frac{cm^2}{s}$ (dry Nylon at room temperature) we get $\ell = 0.0016\ cm$. Even the thin Kapton flat cables are thick compared to this. Numerical evaluation of equation 7 shows that 90% of the saturation flux is reached for a production depth of about $3 \cdot \ell$.

Figure 3 shows Radon concentration profiles calculated for a thin membrane (approximate thickness of the the flat Kapton cables) and various diffusion constants. One can see that for small diffusion constants the profile becomes flat inside the membrane. This makes sense as the unstable

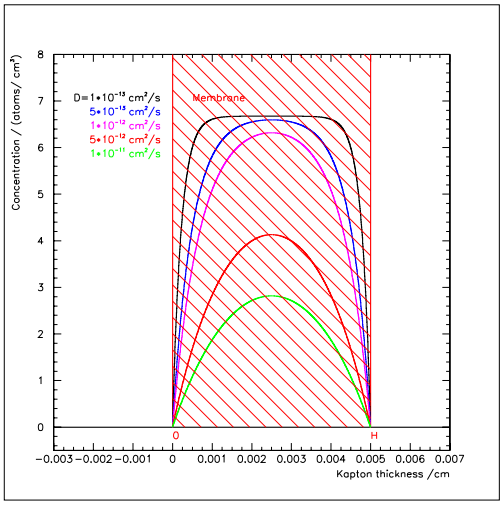

Figure 3: Steady state Radon concentration inside a thin membrane as determined by function 6.

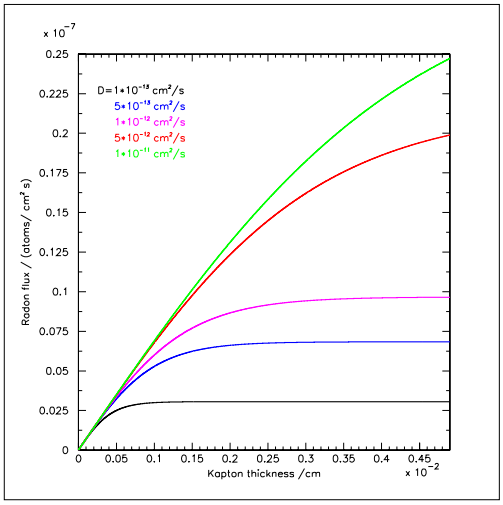

Figure 4: Steady state Radon flux out of a thin membrane, calculated with equation 7.

Radon effectively cannot escape the inner part before decay. With increasing diffusion constant the profile becomes more curved and a thicker layer near the boundaries contributes to the flux. As demanded by the boundary conditions the concentration vanished at the boundaries, independent of diffusion constant and membrane thickness.

Figure 4 shows the Radon flux, as calculated with equation 7. For small diffusion constants the flux goes into saturation, meaning that a thicker membrane will not contribute to the flux as the Radon atoms decay before

reaching the surface. In cases where the diffusion length is much larger than the membrane thickness ($\sqrt{\frac{D_i}{\lambda}} \gg H_i$) the Radon outgassing per unit area is simply given by the limiting value of equation 7:

$$\Phi_{i,\infty} \;=\; n_i \cdot \sqrt{\frac{D_i}{\lambda}}. \tag{8}$$

For all practical cases, involving diffusion at cryogenic temperatures, which relevant for EXO-200, equation 8 suffices.
What fraction of the Rn atoms escapes from the thin Kapton cables? In case of thick samples or a small diffusion constant where the emitted Radon flux equals its saturation value and the tabulated material parameters:

$$\begin{aligned} \Phi_{i,\infty} &= \alpha \cdot \rho_i \cdot c_i \cdot \sqrt{\frac{D_i}{\lambda}} \\ &= \frac{\alpha \cdot c_i'}{H_i} \cdot \sqrt{\frac{D_i}{\lambda}}. \end{aligned}$$

The escaping fraction is given by a simple analytic expression by a ratio of lengths:

$$f_i \;=\; \frac{1}{H_i} \cdot \sqrt{\frac{D_i}{\lambda}}$$

These equations will be used to model the Radon release from internal detector components.

3.4 Temperature and Gas Species Dependence of the Diffusivity

The estimation of the Radon outgassing requires diffusivity data for Radon at cryogenic temperatures. It is expected that diffusion rates in plastics are a dramatic function of temperature. Radon diffusivity data at room temperature is available for Acrylic and Teflon. For Kapton the diffusivities of He, Ne, Ar, and Kr are known at room temperature. We thus need to use scaling relations to infer the data needed for this estimate.

The temperature, T, dependence of the diffusion constant is governed by the Arrhenius relationship [3, 6]:

$$D(T) \;=\; D_0 \cdot e^{-E_D/R \cdot T}, \tag{9}$$

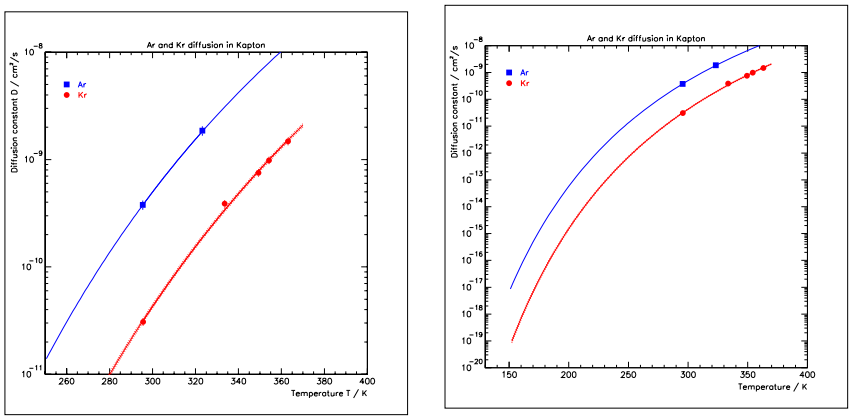

(a) (b)

Figure 5: Temperature dependence of the diffusivities of Ar (blue) and Kr (red)in Kapton as published in [3]. Fig 5(a) shows the temperature range reported in [3]. Fig 5(b) shows the extrapolation to low temperatures.

where D_0 is a reference diffusivity extrapolated from infinite temperature, E_D is the energy of diffusion, and R the ideal gas constant. The few Rn diffusivities reported in the literature are typically measure at room temperature. Internal EXO-200 polymers are held at a temperature of $T = 167\ K$. We thus have to extrapolate experimental diffusivity data over many orders of magnitude to estimate the outgassing yields of those materials at temperatures relevant for EXO-200.
When comparing diffusivities of different gases, it is expected to find an exponential dependence on the effective atomic or molecular diameter, d_e, squared [6]:

$$D(d_e) \;=\; 1\,\frac{cm^2}{s}\cdot e^{k_1+k_2\cdot d_e^2} \;=\; D(T_r), \tag{10}$$

with k_1 and k_2 denoting material dependent constants and assuming that the data was taken at some known reference temperature T_r. Note that [6] uses a parameterization to powers of 10 and not of e as here. Further note that the k_1 and k_2 values reported in table 2 of reference [6] only reproduce the data shown in figure 2 of the same paper if one takes the d_e-values in units of $\mathring{A}$ instead of nm, as stated in [6].
Figure 5 shows our re-analysis of the temperature dependence of Argon and Krypton diffusivities for Kapton, with the data taken from reference [3].

Diffusion energies for Radon are not known for most of the polymers of interest. We are thus forced to estimate E_D values from yet another scaling relation. It has been pointed out in [6] that E_D stands in a linear relation to the squared atomic/molecular diameter, d_e, of the diffusing gas species. Figure 3 of reference [6] shows this linear relation for six different polymers. We can thus use this relation to extrapolate published diffusion energies for stable noble gases to obtain an estimate for Radon. Using a data compilation by S. Pauly of the German Hoechst company, a major manufacturer of polymer films, we obtain diffusion energies for Radon in Acrylic (Poly methyl methacrylate), and FEP [12]. FEP and PTFE (used in EXO-200) are chemically similar but not identical. The former material is melt-processable while the latter is shaped by sintering. FEP was the closest proxy for which diffusivity data could be found. The Kapton estimate was obtained, as stated above, by a re-analysis of the data published in [3]. The diffusion energy for Radon (and with it the Radon diffusion temperature dependence) is obtained from stable noble gas data by fitting to:

$$E_D \;=\; p_1 + p_2 \cdot d_e^2. \tag{11}$$

Substituting equations 9 and 11 into equation 10 and solving for D yields:

$$\begin{aligned} D(T, d_e) &= 1\,\frac{cm^2}{s} \cdot e^{k_1 + k_2 \cdot d_e^2} \cdot e^{\frac{E_D}{R} \cdot \frac{T - T_r}{T \cdot T_r}} \\ &= 1\,\frac{cm^2}{s} \cdot e^{k_1 + k_2 \cdot d_e^2} \cdot e^{\frac{p_1 + p_2 \cdot d_e^2}{R} \cdot \frac{T - T_r}{T \cdot T_r}}, \end{aligned} \tag{12}$$

an expression for the diffusivity of all noble gases at any temperature. Equation 12 allows us to derive temperature dependent Radon diffusivities from data published for stable gases.

Unfortunately Schowalter et al. do not disclose in their paper [3] what system of atomic diameters they used and what lead them to their choice. The Schowalter diffusivities were re-analyzed using three different sets of atomic diameters: those traced out of figure 7 of reference [3], van-der-Waals radii published in [7], and d_e values published in [6]. Figure 6 shows the resulting data sets. As can be seen from figure 6 the arbitrary choice of different systems of (self consistent) atomic diameters leads to a three order of magnitude difference in the estimates for the Radon diffusivity in Kapton. This is not a satisfactory situation. Upon email request C. Connolly, the corresponding author of reference [3], was not interested to explain which atomic sizes were used in their analysis. The following extrapolations are based on the atomic sizes taken from the Teplyakov paper [6] that are at least traceable to published data.

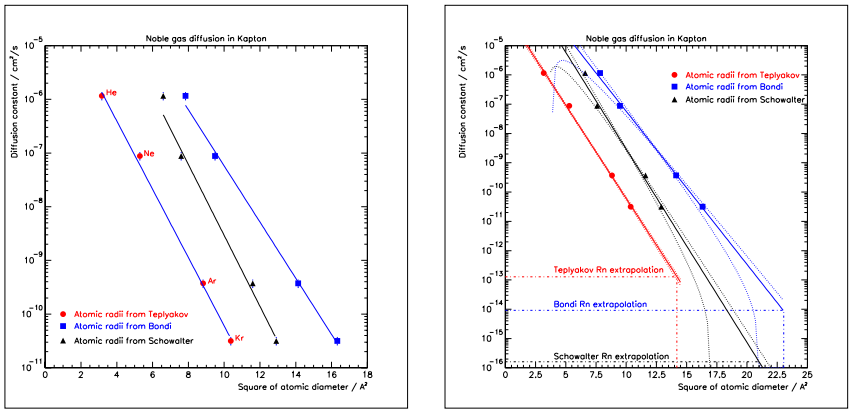

(a) (b)

Figure 6: Dependence of the diffusivities in Kapton on the noble gas species. The data has been taken from [3]. The red, black, and blue symbols in fig 6(a) correspond to the same diffusivities but different atomic radii (taken from [3, 6, 7] respectively). The arbitrary choice of the source of the atomic dimensions results in different parameterizations. Fig 6(b) shows the extrapolation to the Radon atomic size. The choice of different measures of the atomic size clearly lead to very different Radon extrapolations.

Unfortunately, none of the published diffusivities or diffusion energies come with an uncertainty estimate. To obtain at least an estimate of the scatter it is assumed that all data points reported for a certain material have equal error. These equal errors are then adjusted to obtain a reduce χ^2-value of one when fitting the data to equations 9 and 10, serving as an indirect measure of uncertainty.

Figure 7 shows the atomic size systematics of diffusivities and diffusion energies for various polymers as derived from the Hoechst tabulation [12]. From the top panel of figure 7 we see that the diffusivities obtain for stable noble gases do follow systematic trends. The solid lines indicate the fits of D as a function of d_e^2. The dashed lines indicate the Radon extrapolations. For PVC our fit to the Pauly data [12] is compared to the published parameterization by Teplyakov [6] for the same material (black dash dotted line). The two parameterizations seem to be in reasonable agreement. The only data available for FEP is unfortunately not for noble gases but the species indicated in figure 7. The points at the Radon atomic diameter correspond

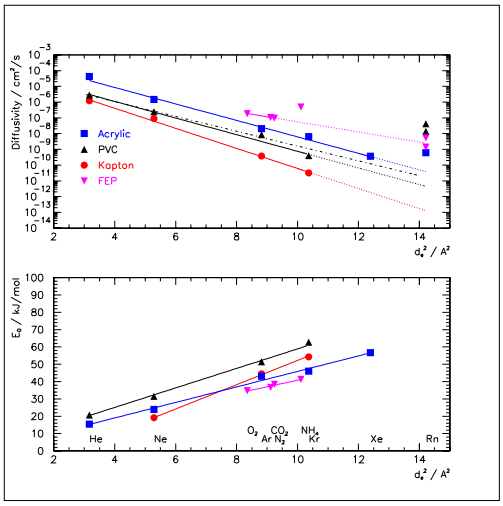

Figure 7: Diffusivity and diffusion energy data found in [12] as a function of the atomic/molecular diameter squared. The solid lines show the fits to the stable noble gas data used to extrapolate to Rn. The dashed-dotted line in the upper panel shows the parameterization for PVC reported in [6]. The dashed lines represent the extrapolation of the stable gas diffusivity data to Radon. Experimental data for Radon is shown where available. These data were not included in the stable-gas fits.

to the few experimental diffusivities that have been published. Except for FEP these do not seem to fit into the overall systematic trends observed for other noble gases. For PVC the mismatch factors (D_{meas}/D_{estim}) range from 3.7 to 28000, depending which reference is used. For acrylic we find a mismatch factor of 16 (relative to [9]), and for FEP of 1.8 and 2.1 (relative to [10, 11]), respectively. Note that the parameterization for PVC, presented here seems to agree reasonably well with that published in reference [6], as can be seen in figure 7. The fact that some measured Radon diffusivities do not seem to fit into the systematics observed for stable noble gases is a warning sign. It could indicate problems with some of the experiments or a strong dependence on the detailed chemical or physical (micro-cracking, porosity etc.) makeup of the samples. As an example: the PVC diffusivities are reported in [12] for unplasticized polymer, while [9] reports two values for *hard* and *soft* PVC. As unsatisfactory as this situation may be, in the absence of relevant data there seems to be no other choice than to rely on these scalings. Given all this one should probably assign an error of plus minus one to the exponent of the diffusivities in a logarithmic scale.

The linear d_e dependence of the diffusion energy, displayed in the lower panel of figure 7, show much smaller scatter than the diffusivities. Here the extrapolation from stable gas data to Radon doesn't span such a large parameter range either. This is probably somewhat more reliable than the extrapolation of (exponential) diffusivities. The Kapton data was supplied by V. Teplyakov, values for all other polymers were derived from data found

Material	p_1 $[\frac{kJ}{mol}]$	p_2 $[\frac{kJ}{mol\ \mathring{A}^2}]$	ρ_p	σ_D/D	$k_1 \cdot 10^4$ $[\mathring{A}^{-2}]$	k_2	ρ_k	σ_D/D	T_R $[K]$	$D(167\ K)$ $[\frac{cm^2}{s}]$	$D(298\ K)$ $[\frac{cm^2}{s}]$	Ref
Kapton	-17.9 ± 0.9	7.0 ± 0.14	-0.96	0.015	1.4 ± 1.0	-1.47 ± 0.10	-0.98	0.27	295	$1.1 \cdot 10^{-24}$	$1.8 \cdot 10^{-13}$	
											$8.6 \cdot 10^{-17}$	[3]
Acrylic	1.12 ± 0.92	4.48 ± 0.20	-0.86	0.044	10.5 ± 6.5	-1.20 ± 0.07	-0.96	0.39	298	$5.1 \cdot 10^{-20}$	$4.0 \cdot 10^{-11}$	
											$6.2 \cdot 10^{-10}$	[9]
FEP	2.88 ± 4.4	3.79 ± 0.48	-1.0	0.02	0.89 ± 0.07	-0.74 ± 0.01	-1.0	0.001	298	$4.0 \cdot 10^{-17}$	$2.5 \cdot 10^{-9}$	
PTFE											$1.4 \cdot 10^{-9}$	[10]
											$5.3 \cdot 10^{-9}$	[11]
PVC	2.58 ± 0.40	5.63 ± 0.11	-1.0	0.02	0.89 ± 0.07	-0.74 ± 0.01	-0.52	0.032	298	$2.1 \cdot 10^{-23}$	$4.6 \cdot 10^{-12}$	
											$1.7 \cdot 10^{-11}$	[6]
											$4.2 \cdot 10^{-8}$	[9]
											$1.4 \cdot 10^{-8}$	[9]
											$1.3 \cdot 10^{-7}$	[13]

Table 3: Compilation of the diffusivity parameterizations for several polymers. p_1 and p_2 denote the parameters of the linear fit of the diffusion energy versus the atomic/molecular diameter squared, as defined in equation 11. ρ_p denotes the error correlation coefficient, and σ_D/D the fractional error assumed for the data to obtain a fit with a reduced $\chi^2 = 1.0$. k_1 and k_2 are the parameters of the fitted diffusivities versus the atomic/molecular diameter squared, as defined in equation 10. ρ_k and σ_D/D have the same meaning as for the previous columns. T_R stands for the reference temperature for which diffusivity data has been reported. Finally, $D(167\ K)$ and $D(298\ K)$ stand for the estimated diffusivities at the respective temperatures. The fit for Kapton was obtained using diffusivity data published in in [3], re-analyzed using atomic diameters from [6]. All other fits were derived from data published in reference [12].

in reference [12]. Table 3 gives a compilation of all parameters required to estimate the diffusivity at EXO-200 relevant temperatures.

4 Yield Estimate

The material amounts and ^{238}U content of the various TPC components, reported in table 1, can now be combined with recoil and diffusion yields, reported in tables 2 and 3, to obtain an estimate for the Radon outgassing into the Xenon. It is assumed that all components contain ^{238}U at the limit determined by the pre-installation analysis. No errors are given as the determination of the diffusivities and their temperature dependence has to be considered semi-quantitative. For all internal parts the components' total surface area has been used. For external copper parts the surface area was divided by two to account for the fact that the Xenon only wets one side. Screws were excluded from the phosphor bronze accounting as it is unclear what fraction of their surface area is in contact with the Xenon. Table 4

Component	Recoil yield $\left[\frac{atoms}{d}\right]$	Diffusion yield $\left[\frac{atoms}{d}\right]$	
		$T = 167\ K$	$T = 298\ K$
Flat cables (Kapton)	0.71	$6.6 \cdot 10^{-6}$	2.7
Acrylic	$1.2 \cdot 10^{-4}$	$5.5 \cdot 10^{-6}$	0.16
Teflon	$9.1 \cdot 10^{-5}$	$1.8 \cdot 10^{-4}$	1.5
APDs	$4.9 \cdot 10^{-4}$		
External copper	$4.9 \cdot 10^{-4}$		
Internal copper	$3.1 \cdot 10^{-4}$		
Phosphor bronze	$7.2 \cdot 10^{-4}$		
Sum	0.71	$1.9 \cdot 10^{-4}$	4.4
Number of atoms supported in Xe steady state	3.9	$1.0 \cdot 10^{-3}$	243

Table 4: Calculated Radon outgassing.

lists the calculated Radon outgassing by the various TPC components. At an operating temperature of 167 K the Radon outgassing of the TPC cannot support a steady state population of 200 Radon atoms. However, at room temperature it could. This shows the importance of a proper temperature correction of the diffusivity data and points at a concern for a room-temperature full EXO. For a room temperature Xenon detector care

will have to be taken to fully understand the background impact and migration of Radon released by internal components. The use of Kapton based flat cables would probably have to be re-considered.
The question of the error intervals for these estimates is difficult to answer. Many of the measurements used to construct the model presented here were published without any error estimate. For most of the TPC materials only limits are known for their U-content. The conversion of U-concentrations into a Radon decay rates involves the equilibrium assumption, which is experimentally untested. The parameter scalings sometimes span many orders of magnitude, making them vulnerable to uncertainty. All this said, one should probably divide the yields by a factor 10 and multiply them by a factor ten to construct an error interval. However, even in the presence of such large variations, it seems clear that the observed number of Radon atoms in EXO's Xenon is not supported by internal components.
The accounting presented here does not cover an important source of Radon atoms: surface radioactivity. A thin layer of U-containing impurities would probably allow *all* of the Radon, born in it, to escape. From this point of view the conclusions drawn here depend on another assumption: namely that all the internal surfaces have been adequately cleaned and no impurities were introduced during installation and transport. At least for the internal Teflon, we are going to test this assumption by means of neutron activation of *as installed* Teflon. The results can then be compared to those derived for cleaned Teflon, any difference would have to be attributed to surface impurities.

Acknowledgment:
This work benefited from numerous valuable discussions with Peter Rowson. We would like to thank Dr. V. Teplyakov for supplying some the diffusivity estimates and useful clarifications regarding the data in his papers.

References

[1] H. Simgen, talk at LowNu 2002, 3rd International Workshop on Low energy Solar Neutrinos, Heidelberg (2002).

[2] M. Wojcik, W. Wlazlo, G. Zuzel, and G. Heusser, Nuclear Instruments and Methods A 449 (2000) 158.

[3] S.J. Schowalter, C.B. Connolly, and J.M. Doyle, Nuclear Instruments and Methods A 615 (2010) 267.

[4] G. Zuzel et al., Nucl. Inst. Meth. A 498 (2003) 240.

[5] DEAP-CLEAN online Radon data base, http://deapclean.org/radon/

[6] V. Teplyakov and P. Maeres, Gas Separation and Purification 4 (1990) 66.

[7] A. Bondi, Journal of Physical Chemistry 68 (1964) 441.

[8] W. Arafa, Radiation Measurements 35 (2002) 207.

[9] M. Wojcik, Nuclear Instruments and Methods B 61 (1991) 8.

[10] G. Zuzel, private communication (2011).

[11] V. Teplyakov, Vysokomoleculiarnie Soedinenia, Akademia Nauk USSR 26A (1984) 1498.

[12] S. Pauly, Hoechst AG, http://www.dcde.dk/sites/default/files/permeability_and_diffusion_data.p

[13] M. Jiránek et al., Proceedings of the American Association of Radon Scientists and Technologists 2008 International Symposium Las Vegas (NV) (2008)